ACS APPLIED ELECTRONIC MATERIALS

pubs.acs.org/acsaelm

Article

GaN Single Nanowire p−i−n Diode for High-Temperature Operations

Xinbo Zou,*,§ Xu Zhang,§ Yu Zhang, Qifeng Lyu, Chak Wah Tang, and Kei May Lau*

Cite This: https://dx.doi.org/10.1021/acsaelm.9b00801 Read Online

ACCESS | Metrics & More | Article Recommendations

ABSTRACT: III-Nitride single nanowire (NW)-based p−i−n diode was fabricated using a top−down etching method and its electrical and optoelectronic characteristics were investigated from room temperature to high operation temperatures up to 150 °C. The NW p−i−n diode exhibited good rectifying *I*−*V* properties at all measurement temperatures and the forward current could be further enhanced when the temperature was increased. Simulation-based data fitting revealed that the enhanced conduction was a result of increased carrier concentration inside the NW, especially holes in the drift layer, as well as reduced contact resistance. The reverse leakage current was kept low even at elevated temperatures so that the UV (∼365 nm) responsivity remained high for a wide temperature range, suggesting the feasibility of NW p−i−n diode for rectifying purposes and UV photon detection applications in high-temperature environments.

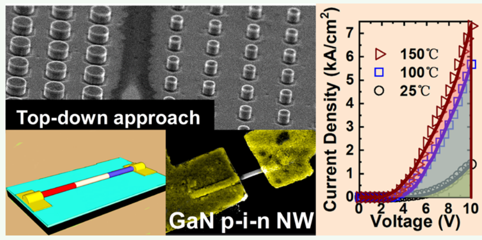

KEYWORDS: *GaN, p−i−n diode, nanowires, high temperature, TCAD simulation, top−down method, UV detection*

■ INTRODUCTION

The use of III-nitride (III-N) semiconductor materials for various energy-efficient optoelectronic and electronic devices has been extensively investigated due to III-N's wide energy band gap, high critical electrical field, and good thermal stability.[1−6] GaN p−i−n diode is a fundamental and important device for a number of applications, such as rectifiers, photodetectors (PDs), microwave switches, solar cells, and so on.[7−10] There has been tremendous progress in recent years on thin film-based GaN p−i−n diodes on native GaN substrates and foreign substrates.[11−13] Despite outstanding device performance obtained for GaN p−i−n diodes grown on native GaN substrates, bulk GaN substrates with low-defect density are still expensive and only available in small sizes, limiting their use for volume productions. GaN p−i−n diodes grown on foreign substrates, such as Si and sapphire, show dislocation density in the range of 10^6−10^9/cm^2, depending on the lattice constant mismatch level, thin film thickness, and growth methods.[8,14,15] Wide energy band gap III-N materials are also promising for monitoring and detecting signals in high-temperature environments,[16,17] such as furnaces, combustion chambers, and so on. However, the defects may deteriorate the device performance at high temperatures.

It is therefore imperative to synthesize and fabricate GaN p−i−n devices out of nanostructures,[5,18−21] which are expected to have low or zero dislocations inside by virtue of their nanoscale dimension.[22−24] In addition, the one-dimension configuration of nanowire (NW) p−i−n diode offers a direct and confined carrier path for carrier transport inside the device under either forward or reverse bias.

The growth and characterization of GaN NW pn junctions have been extensively studied. GaN nanorod pn junctions grown on (111) Si substrates by plasma-assisted molecular beam epitaxy (PA-MBE) were transferred onto a SiO_2/Si substrate to investigate their photoresponse.[5,25] In 2010, p−i−n junction GaN nanowire ensembles were synthesized and fabricated for visible−blind photodetectors.[26] The electrical characteristics of individual GaN p−n junction were measured by current−voltage (*I*−*V*) and electron beam induced current (EBIC), which demonstrated the presence of space charge limited current inside the NW.[19] InN homogeneous p−i−n nanowires were grown on Si substrates and exhibited promising performance for solar cell applications.[27]

An alternative way to fabricate GaN NW devices is the "top−down" method, which starts from GaN layer structures and utilizes etching tools to form nanoscale devices.[28−30] A number of device types have been demonstrated using this scheme, including laser,[31,32] light-emitting diode (LED),[33] and transistor.[29,34−38] There are a number of features for the NW formed by the top−down approach. In addition to high crystalline quality, the NW shares exactly the same epitaxial materials as the starting thin film structure, presents control-

Received: December 6, 2019
Accepted: February 28, 2020
Published: February 28, 2020

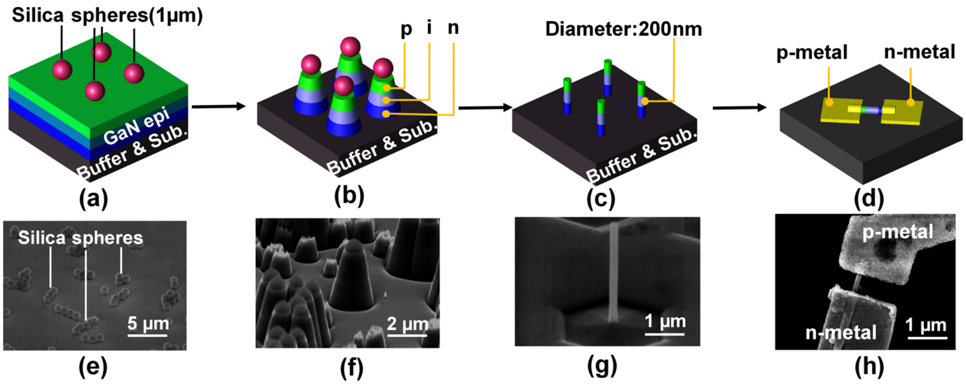

Figure 1. (a–d) Process flow of GaN single NW p–i–n diode using a top–down etching method. (e–h) Corresponding scanning electron microscopy (SEM) images after each fabrication step.

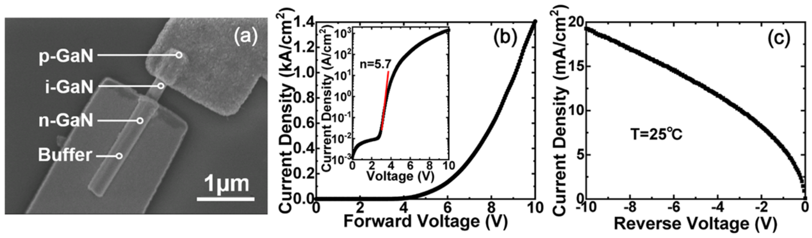

Figure 2. (a) SEM image of NW p–i–n diode. I–V characteristics of NW p–i–n diode under (b) forward and (c) reverse bias.

lable radial dimension by etching time, and is free of the residual substance at the NW sidewall.[29,39]

In this context, single GaN NW p–i–n diode has been fabricated using a top–down etching scheme, starting from the GaN thin film grown on a sapphire substrate. With a radius of 100 nm and drift layer thickness of 500 nm, the GaN NW p–i–n diode showed good rectifying performance at 25 °C and elevated temperature steps up to 150 °C. Technology computer-aided design (TCAD) simulation tools were employed to understand the carrier distribution and transport behaviors inside the nanoscale device. The NW p–i–n diode also showed high responsivity to UV light even at high temperatures, showing its capability of working as a rectifier and UV detector in harsh environments.

■ EXPERIMENTS AND METHODS

Figure 1 illustrates the steps of fabricating single NW p–i–n diode from GaN p–i–n epitaxial layers. The GaN p–i–n layers were grown on a sapphire substrate using low-temperature grown GaN layer as a seed layer and an unintentionally doped GaN layer as a buffer layer. On top of the buffer layer, the p–i–n device structure was grown, consisting of a 1 μm-thick Si-doped n-GaN layer ($\sim n = 2 \times 10^{18}$ cm^{-3}), a 500 nm-thick undoped i-GaN layer, and a 500 nm-thick Mg-doped p-type GaN ($\sim p = 2 \times 10^{17}$ cm^{-3}).

The NW fabrication process started from placing silica spheres (1 μm in diameter) on the GaN p–i–n thin film surface. Then, the GaN layers were etched by inductively coupled plasma etching (ICP) using the silica spheres as etching masks to form micron-sized GaN rods (Figure 1b), which would be further shrunk in an alkaline solution (AZ400K, 85 °C) to form vertical nanowires (Figure 1c). Upon wet-etching in AZ400K, the nanowire with a desired radial dimension was obtained, and simultaneously, the damaged sidewall was eliminated from the nanowire, leaving a smooth surface for further nanowire harvest and metal deposition. Lastly, the vertical nanowires, which had the same doping profile as the initial p–i–n film, were transferred onto a SiO_2/Si substrate. After E-beam lithography, metal deposition, and lift-off, patterned metals were annealed to form contacts: 75/75 nm Ni/Au, 4 min 570 °C annealing in air for p-contact and 75/75 nm Ti/Au, 2 min 500 °C annealing in nitrogen for n-contact. Figure 1e–h shows the corresponding SEM pictures for each key fabrication step.

Measurements of the p–i–n diode's I–V curves were performed at room temperature and elevated temperatures up to 150 °C using the voltage sweep mode from −10 to 10 V, while the substrate was at a floating potential. For UV detection measurements, UV light sources (365 nm) were employed to illuminate the NW p–i–n diode at various power densities. A well-calibrated Si-based photodetector was utilized to monitor the power density of UV light illuminated on the NW diode so that the photoresponse could be further quantitatively analyzed.

■ RESULTS AND DISCUSSION

Figure 2a shows an image of the fabricated NW p–i–n diode, whose p-region and n-region are covered by its contact metal while the i-region was exposed to outer ambience. The nanowire used in this study was uniform in diameter and the metal contacts covered the top half of the p-region and the n-region. As shown in Figure 2b,c, the NW p–i–n diode shows good rectifying I–V characteristics at room temperature. When forward biased, the NW p–i–n diode showed a turn-on voltage of 3.6 V at a current density of 1 A/cm^2. The turn-on voltage matches well with the energy band gap of GaN (3.4 eV). The forward current was exponentially increased as the forward voltage, and the ideality factor was determined to be 5.7, which is larger than the number typically obtained for thin film-based p–i–n diodes (2 to 3). The relatively large ideality factor was correlated to the large contact resistivity that occurred at the semiconductor/metal interface, especially at a low bias range. In a separate experiment where the metal contact was deposited onto a pure p-type nanowire, the average specific contact resistivity was determined to be around several Ω·cm^2 with bias smaller than 0.5 V.

Despite the large ideality factor at a low bias range, the forward current density could reach 1.4 kA/cm^2 at a forward bias of 10 V, and the corresponding specific on-resistance was as small as 2.52 mΩ·cm^2. The low differential on-resistance was

https://dx.doi.org/10.1021/acsaelm.9b00801
ACS Appl. Electron. Mater. XXXX, XXX, XXX−XXX

a result of carrier injection from the two terminals of the diode as well as conductivity modulation. The reverse leakage current density of NW p−i−n diode was only 20 mA/cm^2 at a relatively large reverse bias of −10 V. The leakage current density was much smaller compared with some GaN NW p−i−n diodes in the literature,[19,21,40,41] partly due to the absence of residual materials on the sidewall of the NW device using a top−down approach. The on/off current ratio (±10 V) was determined to be around 7 × 10^4 at 25 °C.

The electrical characteristics of NW p−i−n diode at various temperature steps are shown in Figure 3. Figure 3a,b illustrates

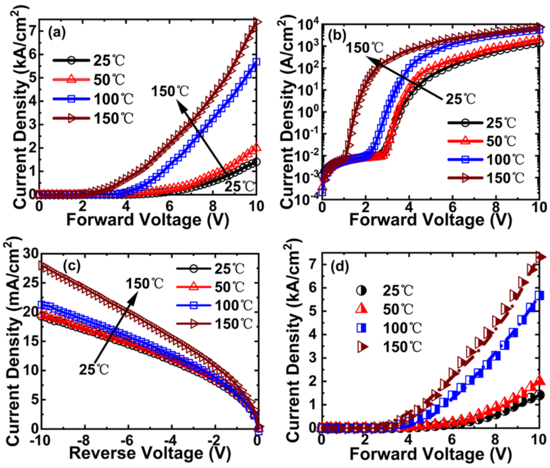

Figure 3. $I-V$ characteristics of NW p−i−n diode at various temperatures in (a) linear scale and (b) logarithmic scale. (c) Leakage current density at various temperature steps. (d) Measured $I-V$ characteristics (dash dot line) and corresponding data fitting curves (half-open symbols).

the current−voltage ($I-V$) characteristics of the NW diode at various temperatures from 25 to 150 °C in linear scale and logarithmic scale, respectively. As the temperature rose, an increase in forward current was observed. Given the 1 A/cm^2 current standard, the threshold voltage was gradually reduced from 3.6 to 1.55 V, while the ideality factor was also significantly improved from 5.7 at 25 °C to 2.3 at 150 °C. The differential on-resistance of the NW was calculated to be only 0.58 mΩ·cm^2 at 150 °C and the reverse leakage current was still kept as low as 28 mA/cm^2 at high temperatures.

To understand NW p−i−n diode's temperature-dependent $I-V$ behaviors, a simulation-based data fitting was performed using the TCAD simulation tool. Simulated $I-V$ electrical characteristics of the NW diode at four different temperature steps are shown in Figure 3d, where all of the simulation results matched well with the measurement results. The GaN physical parameters used in this simulation such as electron affinity, carrier lifetime, carrier mobility,[42] and specific contact resistance are summarized in Table 1[42,43]

From the simulation-based $I-V$ fitting, two mechanisms that were responsible for the improved NW conduction were revealed: enhanced carrier concentration in the drift region and reduced contact resistance.

Figure 4 illustrates the simulated carrier distribution along the NW z-axis at various temperatures at a fixed forward voltage of 3 V. At high temperatures, the electron−hole concentration product at equilibrium state would be considerably increased so that the minority carrier concentration on either side of the junction would be augmented

Table 1. Parameters Used in Temperature-Dependent GaN NW Device $I-V$ Simulations

parameters	quantity	unit	description
E_g (25 °C)	3.46	eV	direct band gap at 25 °C
affinity	4.1	eV	electron affinity
Con.resist (25 °C)	27	mΩ·cm^2	average contact resistivity at 25 °C
Con.resist (50 °C)	19.6	mΩ·cm^2	average contact resistivity at 50 °C
Con.resist (100 °C)	4.7	mΩ·cm^2	average contact resistivity at 100 °C
Con.resist (150 °C)	3	mΩ·cm^2	average contact resistivity at 150 °C
Mun1	100	cm^2/V·s	arora low field mobility model parameter
Mup1	12	cm^2/V·s	
Mun2	1200	cm^2/V·s	
Mup2	145	cm^2/V·s	
Alphan.arora	−1.5		
Alphap.arora	2		
Betan.arora	−1.5		
Betap.arora	−2.34		
Taun0 (25 °C)	0.7 × 10^{-9}	s	electron lifetime at 25 °C
Taup0 (25 °C)	2 × 10^{-9}	s	hole lifetime at 25 °C
Augn (25 °C)	3 × 10^{-31}	cm^6/s	Auger recombination parameter for electron at 25 °C
Augp (25 °C)	3 × 10^{-31}	cm^6/s	Auger recombination parameter for hole at 25 °C
EDB	0.017	eV	dopant activation energies for donor
EAD	0.160	eV	dopant activation energies for acceptor

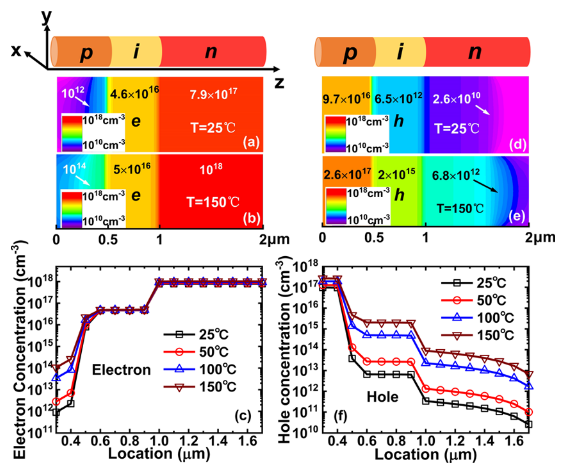

Figure 4. Extracted carrier information at forward bias of 3 V: electron concentration distribution along the axis of p−i−n diode at (a) 25 °C and (b) 150 °C. Hole concentration distribution along the axis of p−i−n diode at (d) 25 °C and (e) 150 °C. Extracted (c) electron and (f) hole concentration along the z-axis at various temperature steps.

according to the Shockley boundary conditions, as verified by the simulation results of Figure 4c,f. The theoretical calculations also suggested that the electron distribution in the drift region typically remained the same, whereas the hole concentration was greatly enhanced with increasing temperatures.

Another factor that would help promote the forward current was the reduction of contact resistance at higher temperatures.

https://dx.doi.org/10.1021/acsaelm.9b00801
ACS Appl. Electron. Mater. XXXX, XXX, XXX−XXX

In a separate experiment, pure p-GaN and n-GaN nanowires were also fabricated to measure the pure p-type and n-type nanowire conductivity at various temperatures, as shown in Figure 5. It was found that the conductivity was greatly

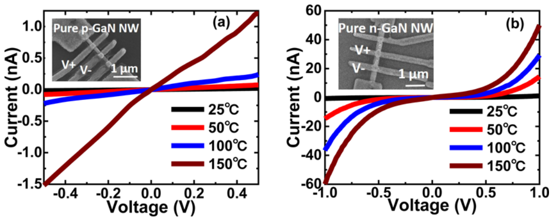

Figure 5. *I*−*V* characteristics of pure (a) p-GaN and (b) n-GaN NW at various temperature steps using two-terminal measurement methods.

improved as the temperature for both NWs was increased. Due to the relatively larger activation energy of Mg dopant in p-GaN compared to that of the Si dopant in n-GaN, most of the Si dopants have already been activated at room temperature, while a considerable portion of the Mg dopants can only be activated at a higher temperature. With a higher hole concentration at a high temperature, a better metal/p-GaN contact was thus obtained. For n-type GaN NW, the current was increased sharply for $V > 0.5$ V, indicating a shallow barrier for the metal/NW contact, leading to a nonideal ohmic contact. The differential on-resistance was greatly reduced from a few m$\Omega\cdot$cm^2 to several m$\Omega\cdot$cm^2 for $V > 0.5$ V. From the simulation-based data fitting process, it was also found that a reduction of average contact resistivity of the NW from 27 m$\Omega\cdot$cm^2 at 25 °C to 3 m$\Omega\cdot$cm^2 at 150 °C could well reproduce the *I*−*V* characteristics.

Figure 6a shows the *I*−*V* characteristics of the NW diode in dark condition and under UV light (λ = 365 nm) illumination.

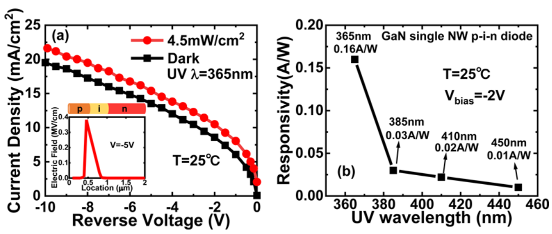

Figure 6. (a) Reverse current density of GaN single NW p−i−n diode in dark environment and under UV light (365 nm) illumination. (b) Wavelength-dependent responsivity of NW p−i−n diode at a reverse bias of −2 V.

An input UV light intensity of 4.5 mW/cm^2 on the NW detector yielded a photocurrent density of 2.08 mA/cm^2, corresponding to a responsivity of 160 mA/W at −10 V and quantum efficiency of 54.1%. Further calculation revealed that quite a uniform responsivity (150 ± 30 mA/W) was obtained for the NW device under a wide range of bias up to −10 V, measured under 4.5 mW/cm^2 365 nm UV light illumination.

The measured responsivity of the NW photodiode was much higher than that of the thin film p−i−n diode (15 mA/W) using the same epitaxial structure. This is because photons from the UV sources could be directly absorbed by the drift region of the NW device while there existed a significant optical loss of photons in the path for thin film p−i−n diodes, e.g., the light absorption in the p-GaN layer when used as a front-illuminated PD. In addition to the absence of optical loss in the optical path, another advantage of using nanowires as a UV photodetector was that the electrical field inside the NW under reverse bias was uniform along the radial direction (*xy*-plane of Figure 4) and the peak electrical field was observed at the p−i interface, which is designed to be exposed to UV light for detection purpose. It should be noted that the surface depletion effects, which have been observed for extremely small nanowires,[44] have not been included in this study, partly because the diameter was relatively large and the surface effects have not been noticeably measured through substrate potential alternation. The cut-off wavelength was found to be around 365 nm, which matches the direct energy band gap (3.4 eV) of the GaN material. The NW PD also demonstrated a good selectivity of UV (365 nm) to visible (450 nm) light, which was measured to be about 16:1, much higher than that using relatively narrower energy band gap materials.

Figure 7 shows the *I*−*V* characteristics of the fabricated GaN NW p−i−n diode in dark environment and under UV light

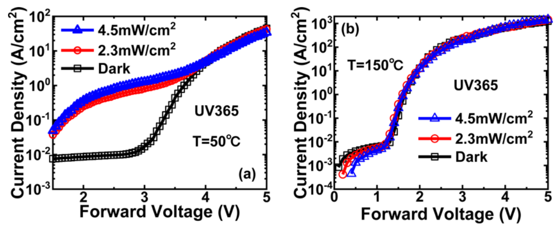

Figure 7. Forward *I*−*V* characteristics of NW diode in dark environment and under UV light (365 nm) illumination at (a) 50 °C and (b) 150 °C.

illumination at 50 and 150 °C. As shown in Figure 6a, at 50 °C, the current of the NW diode at a low bias range (2−3 V) was greatly enhanced under UV illumination, which could be attributed to extra carriers in the drift layer induced by the UV light illumination. As a result, the threshold voltage of the NW diode at 1 A/cm^2 was reduced from 3.65 V in dark environment to 3.25 and 2.75 V under UV light illumination of the power density of 2.3 and 4.5 mW/cm^2, respectively.

While at 150 °C, the forward characteristics for the NW diode in dark and under UV light illumination tend to overlap with each other for nearly the entire measurement bias range. This could mean that the relatively weak UV illumination level presented an insignificant effect on the current level and the turn-on voltage, as the high temperature of 150 °C had already boosted the carrier concentration and improved the contact resistivity.

When the NW diode was reverse biased at 50 °C, the responsivity of the diode (−5 V) was determined to be 212 mA/W with a 365 nm UV power density of 2.3 mW/cm^2. As the temperature was elevated to 150 °C, both dark current and photocurrent was increased, as summarized in Table 2. The responsivity and corresponding quantum efficiency of the NW at −5 V was further enhanced up to 238 mA/W and 95.2%. The elevated responsivity at high temperature mainly arises from the increased density-of-states of the conduction band, which thus promotes the transition rate of photon absorption as well as photoresponse.[45]

■ CONCLUSIONS

Single nanowire-based III-nitride p−i−n diode was fabricated using a top−down etching method. The fabricated nanowire

https://dx.doi.org/10.1021/acsaelm.9b00801
ACS Appl. Electron. Mater. XXXX, XXX, XXX−XXX

Table 2. Measured Current Density in Dark and Under UV Illuminations at 50 and 150 °C

temperature (°C)	reverse voltage (V)	current in dark (mA/cm^2)	current with UV 365 nm, 4.5 mW/cm^2 (mA/cm^2)
50	−3	10.10	12.79
	−5	13.18	15.94
150	−3	13.31	16.42
	−5	17.84	20.94

featured a diameter of 200 nm and retained exactly the same p−i−n structure along the axial direction as the initial GaN p−i−n epitaxial thin film. At 25 °C, the NW p−i−n diode exhibited good rectifying *I*−*V* characteristics with a turn-on voltage of 3.6 V at 1 A/cm^2 and leakage current as low as 7.4 pA at −10 V. The ideality factor was extracted as 5.7 and the forward current density could reach 1.4 kA/cm^2 at 10 V. The NW diode is also promising for high-temperature operations as rectifiers and UV photodetectors. The forward conduction was improved as the temperature was increased up to 150 °C, while the reverse leakage current was only slightly increased due to the wide energy band gap of the GaN materials. The NW presented good UV (∼365 nm) detection for a wide temperature range that the responsivity was measured to be around 160 and 238 mA/W at 25 and 150 °C, respectively. The top−down etching approach and characteristics of GaN NW p−i−n diode paved a promising path for its use in high-temperature and harsh environments.

AUTHOR INFORMATION

Corresponding Authors

Xinbo Zou − *ECE Department, Hong Kong University of Science and Technology, Kowloon 999077, Hong Kong; School of Information Science and Technology, ShanghaiTech University, Shanghai 201210, China;* orcid.org/0000-0002-9031-8519; Email: zouxb@shanghaitech.edu.cn

Kei May Lau − *ECE Department, Hong Kong University of Science and Technology, Kowloon 999077, Hong Kong;* Email: eekmlau@ust.hk

Authors

Xu Zhang − *ECE Department, Hong Kong University of Science and Technology, Kowloon 999077, Hong Kong*

Yu Zhang − *School of Information Science and Technology, ShanghaiTech University, Shanghai 201210, China*

Qifeng Lyu − *ECE Department, Hong Kong University of Science and Technology, Kowloon 999077, Hong Kong*

Chak Wah Tang − *ECE Department, Hong Kong University of Science and Technology, Kowloon 999077, Hong Kong*

Complete contact information is available at: https://pubs.acs.org/10.1021/acsaelm.9b00801

Author Contributions

[§]X. Zou and X. Zhang contributed equally to this work.

Notes

The authors declare no competing financial interest.

ACKNOWLEDGMENTS

This work was supported in part by RGC General Research Fund under Grant No. 16213915, Shanghai Pujiang Program under Grant No. 18PJ1408200, ShanghaiTech Startup Fund, and Shanghai Eastern Scholar (Youth) Program.

REFERENCES

(1) Ji, M.; Kim, J.; Detchprohm, T.; Zhu, Y.; Shen, S.; Dupuis, R. D. p-i-p-i-n Separate Absorption and Multiplication Ultraviolet Avalanche Photodiodes. *IEEE Photonics Technol. Lett.* **2018**, *30*, 181−184.

(2) Siddique, A.; Ahmed, R.; Anderson, J.; Nazari, M.; Yates, L.; Graham, S.; Holtz, M.; Piner, E. L. Structure and Interface Analysis of Diamond on an AlGaN/GaN HEMT Utilizing an in Situ SiNx Interlayer Grown by MOCVD. *ACS Appl. Electron. Mater.* **2019**, *1*, 1387−1399.

(3) Liu, D.; Fabes, S.; Li, B.-S.; Francis, D.; Ritchie, R. O.; Kuball, M. Characterization of the Interfacial Toughness in a Novel "GaN-on-Diamond" Material for High-Power RF Devices. *ACS Appl. Electron. Mater.* **2019**, *1*, 354−369.

(4) Hua, M.; Cai, X.; Yang, S.; Zhang, Z.; Zheng, Z.; Wang, N.; Chen, K. J. Enhanced Gate Reliability in GaN MIS-FETs by Converting the GaN Channel into Crystalline Gallium Oxynitride. *ACS Appl. Electron. Mater.* **2019**, *1*, 642−648.

(5) Cuesta, S.; Spies, M.; Boureau, V.; Donatini, F.; Hocevar, M.; den Hertog, M. I.; Monroy, E. Effect of Bias on the Response of GaN Axial p−n Junction Single-Nanowire Photodetectors. *Nano Lett.* **2019**, *19*, 5506−5514.

(6) Kou, J.; Chen, S. H.; Che, J.; Shao, H.; Chu, C.; Tian, K.; Zhang, Y.; Bi, W.; Zhang, Z.; Kuo, H. On the Carrier Transport for InGaN/GaN Core-Shell Nanorod Green Light-Emitting Diodes. *IEEE Trans. Nanotechnol.* **2019**, *18*, 176−182.

(7) Liu, W.; Xu, W.; Zhou, D.; Ren, F.; Chen, D.; Yu, P.; Zhang, R.; Zheng, Y.; Lu, H. Avalanche Ruggedness of GaN p-i-n Diodes Grown on Sapphire Substrate. *Phys. Status Solidi A* **2018**, *215*, No. 1800069.

(8) Zheng, B. S.; Chen, P. Y.; Yu, C. J.; Chang, Y. F.; Ho, C. L.; Wu, M. C.; Hsieh, K. C. Suppression of current leakage along mesa surfaces in GaN-based p-i-n diodes. *IEEE Electron Device Lett.* **2015**, *36*, 932−934.

(9) Ohta, H.; Kaneda, N.; Horikiri, F.; Narita, Y.; Yoshida, T.; Mishima, T.; Nakamura, T. Vertical GaN p-n Junction Diodes With High Breakdown Voltages Over 4 kV. *IEEE Electron Device Lett.* **2015**, *36*, 1180−1182.

(10) Chen, W.; Wong, K.-Y.; Huang, W.; Chen, K. J. High-performance AlGaN/GaN lateral field-effect rectifiers compatible with high electron mobility transistors. *Appl. Phys. Lett.* **2008**, *92*, No. 253501.

(11) Zou, X.; Zhang, X.; Lu, X.; Tang, C. W.; Lau, K. M. Fully Vertical GaN p-i-n Diodes Using GaN-on-Si Epilayers. *IEEE Electron Device Lett.* **2016**, *37*, 636−639.

(12) Kizilyalli, I. C.; Edwards, A. P.; Nie, H.; Bour, D.; Prunty, T.; Disney, D. 3.7 kV vertical GaN PN diodes. *IEEE Electron Device Lett.* **2014**, *35*, 247−249.

(13) Kizilyalli, I. C.; Prunty, T.; Aktas, O. 4-kV and 2.8-mohm cm2 Vertical GaN p-n Diodes With Low Leakage Currents. *IEEE Electron Device Lett.* **2015**, *36*, 1073−1075.

(14) Zou, X.; Zhang, X.; Lu, X.; Tang, C. W.; Lau, K. M. Fully vertical GaN p-i-n diodes Using GaN-on-Si Epilayers. *IEEE Electron Device Lett.* **2016**, *37*, 636−639.

(15) Zhang, Y.; Wong, H. Y.; Sun, M.; Joglekar, S.; Yu, L.; Braga, N. A.; Mickevicius, R. V.; Palacios, T. In *Design Space and Origin of Off-State Leakage in GaN Vertical Power Diodes*, 2015 IEEE International Electron Devices Meeting (IEDM), December 7−9, 2015; pp 35.1.1−35.1.4.

(16) Hader, J.; Moloney, J. V.; Koch, S. W. Temperature-dependence of the internal efficiency droop in GaN-based diodes. *Appl. Phys. Lett.* **2011**, *99*, No. 181127.

(17) Gür, E.; Tüzemen, S.; Kiliç, B.; Coşkun, C. High-temperature Schottky diode characteristics of bulk ZnO. *J. Phys.: Condens. Matter* **2007**, *19*, No. 196206.

(18) Alloing, B.; Zúñiga-Pérez, J. Metalorganic chemical vapor deposition of GaN nanowires: From catalyst-assisted to catalyst-free growth, and from self-assembled to selective-area growth. *Mater. Sci. Semicond. Process.* **2016**, *55*, 51−58.

(19) Fang, Z.; Donatini, F.; Daudin, B.; Pernot, J. Axial p−n junction and space charge limited current in single GaN nanowire. *Nanotechnology* **2018**, *29*, No. 01LT01.

(20) Park, J. H.; Kissinger, S.; Ra, Y. H.; San, K.; Park, M. J.; Yoo, K. H.; Lee, C. R. Horizontal assembly of single nanowire diode fabricated by p-n junction GaN nw grown by MOCVD. *J. Nanomater.* **2014**, *2014*, No. 951360.

(21) Jacopin, G.; De Luna Bugallo, A.; Rigutti, L.; Lavenus, P.; Julien, F. H.; Lin, Y.-T.; Tu, L.-W.; Tchernycheva, M. Interplay of the photovoltaic and photoconductive operation modes in visible-blind photodetectors based on axial p-i-n junction GaN nanowires. *Appl. Phys. Lett.* **2014**, *104*, No. 023116.

(22) Sankaranarayanan, S.; Kandasamy, P.; Krishnan, B. Catalytic Growth of Gallium Nitride Nanowires on Wet Chemically Etched Substrates by Chemical Vapor Deposition. *ACS Omega* **2019**, *4*, 14772−14779.

(23) Mariana, S.; Gülink, J.; Hamdana, G.; Yu, F.; Strempel, K.; Spende, H.; Yulianto, N.; Granz, T.; Prades, J. D.; Peiner, E.; Wasisto, H. S.; Waag, A. Vertical GaN Nanowires and Nanoscale Light-Emitting-Diode Arrays for Lighting and Sensing Applications. *ACS Appl. Nano Mater.* **2019**, *2*, 4133−4142.

(24) Gómez, V. J.; Santos, A. J.; Blanco, E.; Lacroix, B.; García, R.; Huffaker, D. L.; Morales, F. M. Porosity Control for Plasma-Assisted Molecular Beam Epitaxy of GaN Nanowires. *Cryst. Growth Des.* **2019**, *19*, 2461−2469.

(25) Son, M. S.; Im, S. I.; Park, Y. S.; Park, C. M.; Kang, T. W.; Yoo, K. H. Ultraviolet photodetector based on single GaN nanorod p−n junctions. *Mater. Sci. Eng., C* **2006**, *26*, 886−888.

(26) De Luna Bugallo, A.; Tchernycheva, M.; Jacopin, G.; Rigutti, L.; Henri Julien, F.; Chou, S. T.; Lin, Y. T.; Tseng, P. H.; Tu, L. W. Visible-blind photodetector based on p-i-n junction GaN nanowire ensembles. *Nanotechnology* **2010**, *21*, No. 315201.

(27) Nguyen, H. P. T.; Chang, Y.; Shih, I.; Mi, Z. InN p-i-n Nanowire Solar Cells on Si. *IEEE J. Sel. Top. Quantum Electron.* **2011**, *17*, 1062−1069.

(28) Xu, H.; Hurtado, A.; Wright, J. B.; Li, C.; Liu, S.; Figiel, J. J.; Luk, T. S.; Brueck, S. R. J.; Brener, I.; Balakrishnan, G.; Li, Q.; Wang, G. T. Polarization control in GaN nanowire lasers. *Opt. Express* **2014**, *22*, 19198−19203.

(29) Im, K.-S.; Won, C.-H.; Vodapally, S.; Caulmilone, R.; Cristoloveanu, S.; Kim, Y.-T.; Lee, J.-H. Fabrication of normally-off GaN nanowire gate-all-around FET with top-down approach. *Appl. Phys. Lett.* **2016**, *109*, No. 143106.

(30) Li, Q.; Wright, J. B.; Chow, W. W.; Luk, T. S.; Brener, I.; Lester, L. F.; Wang, G. T. Single-mode GaN nanowire lasers. *Opt. Express* **2012**, *20*, 17873−17879.

(31) Behzadirad, M.; Nami, M.; Wostbrock, N.; Kouhpanji, M. R. Z.; Feezell, D. F.; Brueck, S. R. J.; Busani, T. Scalable Top-Down Approach Tailored by Interferometric Lithography to Achieve Large-Area Single-Mode GaN Nanowire Laser Arrays on Sapphire Substrate. *Acs Nano* **2018**, *12*, 2373−2380.

(32) Li, C. Y.; Wright, J. B.; Liu, S.; Lu, P.; Figiel, J. J.; Leung, B.; Chow, W. W.; Brener, I.; Koleske, D. D.; Luk, T. S.; Feezell, D. F.; Brueck, S. R. J.; Wang, G. T. Nonpolar InGaN/GaN Core-Shell Single Nanowire Lasers. *Nano Lett.* **2017**, *17*, 1049−1055.

(33) Zhang, G.; Li, Z.; Yuan, X.; Wang, F.; Fu, L.; Zhuang, Z.; Ren, F.-F.; Bin, L.; Zhang, R.; Tan, H. H.; Jagadish, C. Single nanowire green InGaN/GaN light emitting diodes. *Nanotechnology* **2016**, *27*, No. 435205.

(34) Fatahilah, M. F.; Yu, F.; Strempel, K.; Römer, F.; Maradan, D.; Meneghini, M.; Bakin, A.; Hohls, F.; Schumacher, H. W.; Witzigmann, B.; Waag, A.; Wasisto, H. S. Top-down GaN nanowire transistors with nearly zero gate hysteresis for parallel vertical electronics. *Sci. Rep.* **2019**, *9*, No. 10301.

(35) Hu, Z.; Li, W.; Nomoto, K.; Zhu, M.; Gao, X.; Pilla, M.; Jena, D.; Xing, H. G. In *GaN Vertical Nanowire and Fin Power MISFETs*, 2017 75th Annual Device Research Conference (DRC), June 25−28, 2017; pp 1−2.

(36) Im, K.-S.; Sindhuri, V.; Jo, Y.-W.; Son, D.-H.; Lee, J.-H.; Cristoloveanu, S.; Lee, J.-H. Fabrication of AlGaN/GaN Ω-shaped nanowire fin-shaped FETs by a top-down approach. *Appl. Phys. Express* **2015**, *8*, No. 066501.

(37) Jo, Y.; Son, D.; Lee, D.; Won, C.; Seo, J. H.; Kang, I. M.; Lee, J. In *First Demonstration of GaN-Based Vertical Nanowire FET with Top-Down Approach*, 2015 73rd Annual Device Research Conference (DRC), June 21−24, 2015; pp 35−36.

(38) Son, D.-H.; Jo, Y.-W.; Seo, J. H.; Won, C.-H.; Im, K.-S.; Lee, Y. S.; Jang, H. S.; Kim, D.-H.; Kang, I. M.; Lee, J.-H. Low voltage operation of GaN vertical nanowire MOSFET. *Solid-State Electron.* **2018**, *145*, 1−7.

(39) Yu, F.; Rümmler, D.; Hartmann, J.; Caccamo, L.; Schimpke, T.; Strassburg, M.; Gad, A. E.; Bakin, A.; Wehmann, H.-H.; Witzigmann, B.; Wasisto, H. S.; Waag, A. Vertical architecture for enhancement mode power transistors based on GaN nanowires. *Appl. Phys. Lett.* **2016**, *108*, No. 213503.

(40) Lu, Y. J.; Lu, M. Y.; Yang, Y. C.; Chen, H. Y.; Chen, L. J.; Gwo, S. Dynamic Visualization of Axial p-n Junctions in Single Gallium Nitride Nanorods under Electrical Bias. *Acs Nano* **2013**, *7*, 7640−7647.

(41) Park, J.-H.; Kissinger, S.; Ra, Y.-H.; San, K.; Park, M.; Yoo, K.-H.; Lee, C.-R. Horizontal Assembly of Single Nanowire Diode Fabricated by p-n Junction GaN NW Grown by MOCVD. *J. Nanomater.* **2014**, *2014*, No. 951360.

(42) Sabui, G.; Parbrook, P. J.; Arredondo-Arechavala, M.; Shen, Z. J. Modeling and simulation of bulk gallium nitride power semiconductor devices. *AIP Adv.* **2016**, *6*, No. 055006.

(43) Silvaco, Inc. Atlas User's Manual. 2016.

(44) Calarco, R.; Marso, M.; Richter, T.; Aykanat, A. I.; Meijers, R.; v.d. Hart, A.; Stoica, T.; Lüth, H. Size-dependent Photoconductivity in MBE-Grown GaN−Nanowires. *Nano Lett.* **2005**, *5*, 981−984.

(45) Sou, I. K.; Ma, Z. H.; Zhang, Z. Q.; Wong, G. K. L. Temperature dependence of the responsivity of II−VI ultraviolet photodiodes. *Appl. Phys. Lett.* **2000**, *76*, 1098−1100.